Article

Effect of ESIPT-Induced Photoisomerization of Keto−Enamine Linkages on the Photocatalytic Hydrogen Evolution Performance of Covalent Organic Frameworks

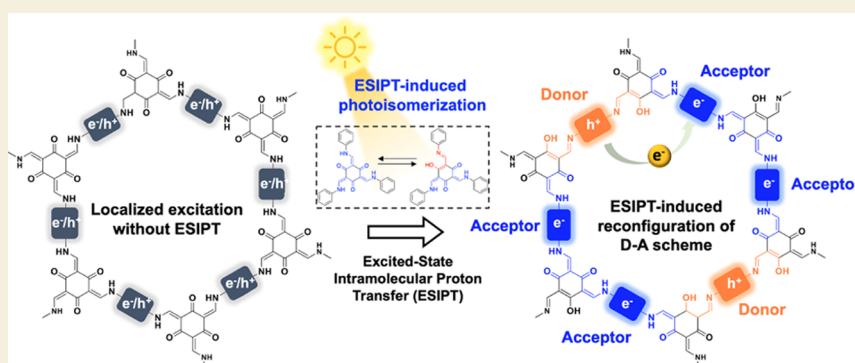Weijun Weng,[§] Zheng Lin,[§] Hualei Zhang, Fushuang Niu, Changchun Wang, Ke Hu,* and Jia Guo*

Read Online

ACCESS | Metrics & More | Article Recommendations | SI Supporting Information

ABSTRACT: Photoexcitation of keto−enamine allows intramolecular proton transfer from C−NH to C=O, leading to tautomerization, while the photogenerated isomers are excluded from the study of photocatalytic applications. Herein, we demonstrate the photoisomerization of keto−enamine linkages on covalent organic frameworks (COFs) induced by excited-state intramolecular proton transfer (ESIPT). Partial enolization generates partially enolized photoisomers with a mixture of keto (C=O) and enol (OH) forms, conferring extended π-conjugation with an increase in electron density. The spatially separated D−A configuration is thus rebuilt with the enol−imine-linked branch as a donor and the keto−enamine-linked branch as an acceptor, and in turn, the photoinduced charges transfer between the two adjacent branches with a long lifetime. We further prove that the partially enolized photoisomer is a key transition instead of the keto−enamine form as an excited-state model to understand the photocatalytic behaviors. Therefore, ESIPT-induced photoisomerization must be considered for rationally designing keto−enamine-linked COFs with enhanced photocatalytic activity. Also, our study points toward the importance of controlling excited-state structures for long-lived separated charges, which is of particular interest for optoelectronic applications.

KEYWORDS: covalent organic frameworks, photocatalysis, proton transfer, H_2 evolution, photoisomerization

INTRODUCTION

Excited-state intramolecular proton transfer (ESIPT) is a classical molecular photoisomerization process that affords a large Stokes shift.[1] Basically, molecules that undergo ESIPT have the thermodynamically favorable enolic form in the ground state. Upon excitation, redistribution of charge density elevates the acidity of the proton donor and the basicity of the proton acceptor simultaneously. This allows the migration of a proton from the donor to acceptor sites, resulting in reversible tautomerization for dual fluorescence emission. Also, the ESIPT can spatially separate the highest occupied and lowest unoccupied molecular orbitals (HOMO and LUMO) to regenerate a donor−acceptor scheme for charge transfer. Although it is highly desirable for photocatalytic conversion, it still remains unexplored.

Two-dimensional covalent organic frameworks (2D COFs) are emerging as a desirable platform for exploring advanced functional materials. They feature 2D periodic atomic frameworks and mutual stacking in a well-defined ordered fashion, thereby producing 1D opening pore channels.[2,3] Through molecular engineering, atomic structure−performance correlation has been established to achieve a series of striking properties for adsorption and separation,[4,5] catalysis,[6−8] energy storage,[9−11] and magnetism.[12] In particular, mounting interest has been aroused for COFs in implementing artificial photosynthesis by converting solar energy into hydrogen in water splitting. Inspired by the design of multichromophoric arrays, a
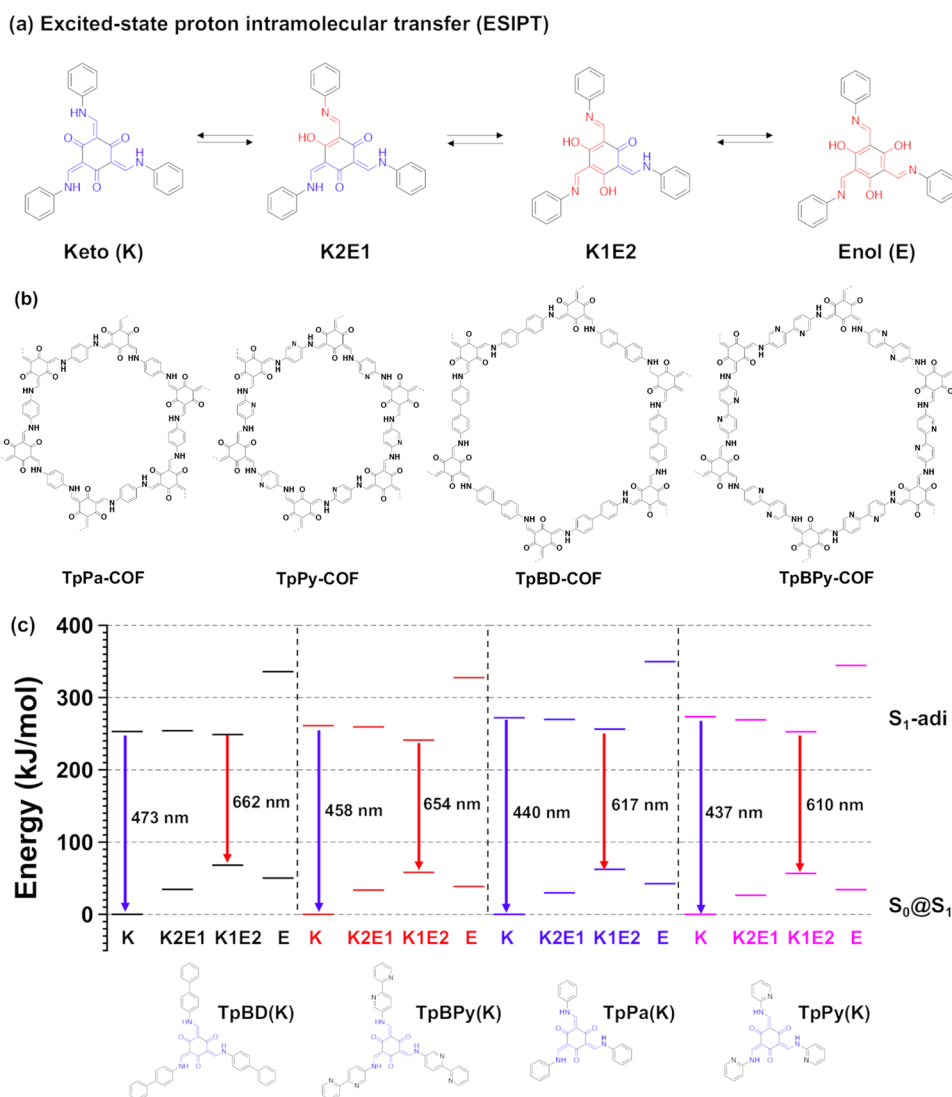
Figure 1. (a) Scheme of the ESIPT process from Keto to transition (K2E1 and K1E2) to Enol forms. (b) Illustration of keto−enamine-linked COFs containing a variety of linkers including phenyl, pyridine, biphenyl, and bipyridine. (c) Relative energy level diagram of the corresponding tautomers after relaxation in the S1 state. S0@S1 represents de-excitation relaxed from the S1 state.

series of heteronuclear photoactive modules such as sulfone,[13] alkyne,[14] benzothiadiazole,[15,16] bipyridine,[17] and triazine[18−20] have been incorporated into COF backbones, constituting extended polygons containing D−π−A multibranches. Such emerging COFs are beneficial to harvest visible light in a broad window and expedite charge transport,[21] thereby outperforming most amorphous or semicrystalline polymers in terms of photocatalytic performances. However, from the photophysical point of view, the photoinduced electron transfer between building blocks at different sites of frameworks is limited by nonconjugated covalent linkages such as keto−enamine, imide, and 1,4-dioxin. Therefore, a study on the photoexcitation state of covalent linkages is of significance, which virtually decides the electron flow direction and charge redistribution, whereas such investigations have rarely been concerned so far.

In this study, we report on ESIPT-induced photoisomerization of keto−enamine linkages for a variety of 2D COFs with different building blocks. In the ground state, keto−enamine linkages render 2D COFs excellent chemical stability due to the irreversible transformation from enol−imine to keto−enamine.[22] In the excited state, the photoisomerization of the keto−

enamine linkage is likely via a reverse ESIPT process. As displayed in Figure 1a, the complete conversion from Keto to Enol is prohibited, as a higher excited-state energy level exists in the Enol form, but partially enolized structures, i.e., K1E2 and K2E1, are thermodynamically stable transitions derived from proton transfer.[23] Our study demonstrates that such ESIPT-induced photoisomerization generates a partially enolized structure with extended conjugation and increased electron density. The spatially separated enol−imine-linked branch and keto−enamine-linked branch serve as a donor and an acceptor, respectively, to accomplish the long-lived charge separation and enhance the photocatalytic conversion efficiency, differing from the case for the Keto isomer and imine-linked analogues. This is the first systematic investigation of excited-state structural transformation of COF-based photocatalysts for a profound insight into photochemical dynamics.

RESULTS AND DISCUSSION

Synthesis of Keto−Enamine-Linked COFs

As displayed in Figure 1b, 1,3,5-triformylphloroglucinol (Tp) was applied to synthesize a variety of keto−enamine-linked
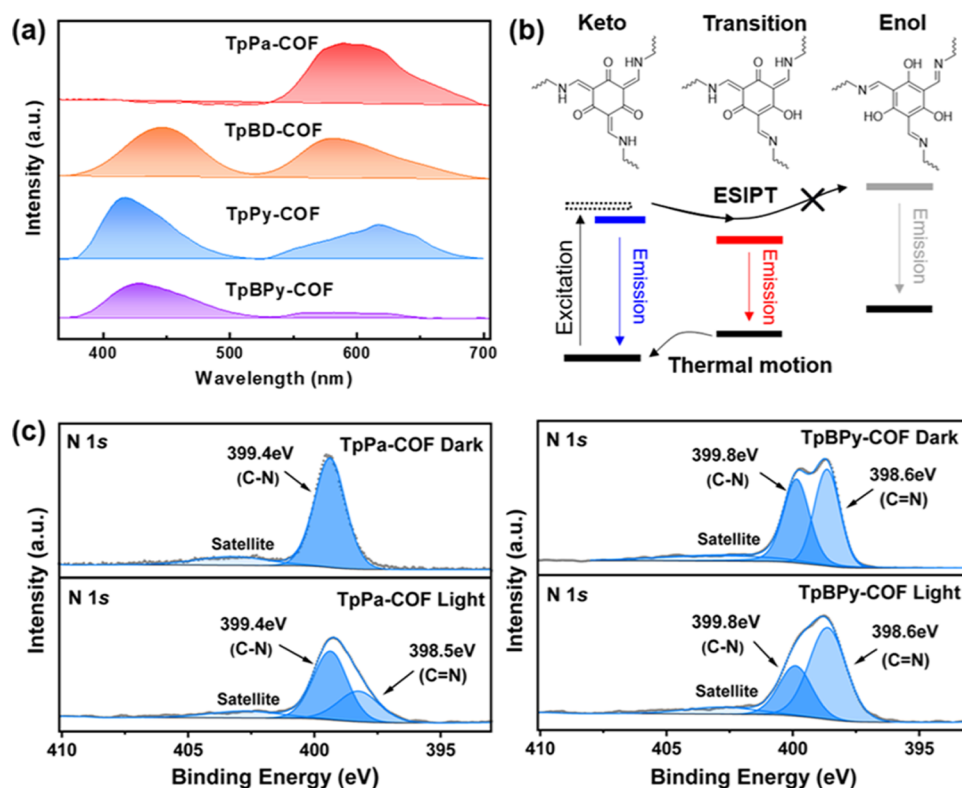
Figure 2. (a) Photoluminescence spectra of TpPa-COF, TpBD-COF, TpPy-COF, and TpBPy-COF. (b) Energy level diagram of ESIPT-induced COF photoisomers. (c) In situ X-ray photoelectron spectra of TpBPy-COF and TpPa-COF in the dark and under visible light ($\lambda > 420$ nm).

COFs, using different diamines with aromatic linkers including phenyl, biphenyl, pyridine, and bipyridine. A general solvothermal synthesis was adopted to undergo an aldimine reaction in mixed solvents at 120 °C for 3 days in the presence of an acetic acid aqueous solution as a catalyst.

The formation of the keto−enamine linkage was proved by various spectroscopic techniques. In the Fourier transform infrared (FT-IR) spectra, the emerging absorbance peaks at 1600 and 1260 cm^{-1} were assigned to C=O and C−NH bonds stemming from the keto−enamine linkages in the COFs (Supporting Information Figure S1). Meanwhile, the solid-state CP/MAS ^{13}C NMR spectra provided evidence for framework formation (Supporting Information Figure S2). The chemical shifts at 182, 144, and 115 ppm could be assigned to the carbons of keto C(a) and enamine C(b) and C(c), respectively, and the other phenyl carbons as well as pyridinic carbons corresponded to the signals in the range of 110−140 ppm.[22,24,25]

Structural characterization was conducted using powder X-ray diffraction (PXRD) and N$_2$ sorption techniques. All of the products were crystalline and gave typical PXRD patterns indexed to the hexagonal 2D COFs (Supporting Information Figure S3). The sharp diffraction peaks at 3.3° are derived from the (100) crystalline facet of TpBPy-COF and TpBD-COF. For TpPa-COF and TpPy-COF with short linkers, the (100) diffraction peaks shifted to 4.7°, which was consistent with the reported X-ray diffraction signal.[26−28] Based on the Scherrer equation, the domain sizes of the crystalline COFs were calculated to be 13.3, 13.4, 11.4, and 12.0 nm for TpBPy-COF, TpBD-COF, TpPa-COF and TpPy-COF, respectively.

The accessible pores of these COFs were assessed by N$_2$ sorption measurement at 77 K. The as-synthesized COFs had high porosity and narrow pore size distributions (Supporting Information Figures S4 and S5). The Brunauer−Emmett−Teller (BET) surface areas were calculated to be 820, 841, 696, and 774 m^{2}g^{-1} for TpBD-COF, TpBPy-COF, TpPy-COF, and TpPa-COF, respectively, and accordingly, the pore volumes were 0.43, 0.41, 0.36, and 0.38 cm^{3}g^{-1}, respectively. Based on the NLDFT method, the pore size of TpBD-COF was determined to be 2.1 nm, identical to that of TpBPy-COF. For the microporous TpPa-COF and TpPy-COF, the pore sizes were around 1−2 nm. Combined with the well-defined PXRD patterns, the results of the N$_2$ sorption measurement indicate that the pores originate from the periodic structures of COFs.

ESIPT-Induced Photoisomerization of Keto−Enamine-Linked COFs

As reported earlier,[29] dual fluorescence emission by single wavelength excitation is responsible for the ESIPT transformation in chromophore molecules. Investigating the photoluminescent property of the keto−enamine-linked COFs can estimate the possibility of an ESIPT-induced tautomerization process.

The study commenced with the computational calculation of model compounds derived from the four COFs. The ESIPT can generate different tautomers by a sequential keto-to-enol transformation, as illustrated in Figure 1c. The excited energy of cutout models and their isomers for the four COFs was calculated by the time-dependent density functional theory (TD-DFT) method at the TD-PBE0-D3BJ/def2-TZVP level. Of the various tautomers, Keto forms possess the most stable ground states (S0). Upon excitation, the structural rearrangement achieves the global minimum of the lowest excited state (S1-adiabatic). As a single proton is transferred, tautomer K2E1 is more stable than the starting form, Keto, giving a small energy decrease in the excited state (1.85 kJ/mol on average). While the

two protons are transferred, the excited energy decreases by 15.23 kJ/mol, indicating that K1E2 is the most stable compared with Keto and K2E1 and causes the long-wavelength fluorescence emission around 600−650 nm (Supporting Information Tables S1−S12). Of the different tautomers, TpBPy (K1E2) has the lowest energy level in the S1 state, implying that the BPy moiety is beneficial to form the stable excited state through partial enolization.

With the theoretical analysis in mind, the fluorescence measurement was conducted for the aqueous dispersions of the four COFs under ambient conditions. As shown in Figure 2a, TpBD-COF and TpPy-COF both show typical dual fluorescence emissions around 410 and 590 nm. This could be interpreted by theoretically predicted ESIPT-induced isomerization (Figure 2b). The short-wavelength emission arises from the Keto form rather than Enol, as the transition from Keto to Enol is thermodynamically prohibited. The long-wavelength emission is attributed to the partially enolized structures, which have low-lying levels in excited states as well as narrowed energy band gaps, resulting in red-shifted emission. Differing from the above two COFs, TpPa-COF exhibited dominant single emission at 600 nm, indicative of remarkable isomerization. In contrast, TpBPy-COF merely emitted blue light at 420 nm. It is most likely that the long-wavelength emission generated by the tautomers of TpBPy-COF is suppressed. From the computational point of view (Supporting Information Tables S1−S12), the calculated HOMO and LUMO of TpBPy(K1E2) are well separated, providing clear evidence that the recombination of photoexcited electron−hole pairs could be effectively weakened. In contrast, TpPa(K1E2) has overlapped molecular orbitals, featuring the HOMO filling many of the gaps in the LUMO and vice versa.

Given the single emission observed from TpPa-COF and TpBPy-COF, the ESIPT-triggered structural transformation was examined via in situ X-ray photoelectron spectroscopy (XPS; Figure 2c). In the dark, the N 1s core level spectrum of TpPa-COF displayed a single peak at 399.4 eV, which could be fitted with the C−N bond of the Keto form.[30] Once TpPa-COF was irradiated by visible light, the N 1s peak was broadened and could be deconvoluted into two peaks at 399.4 and 398.5 eV. The newly emerging peak at 398.5 eV was ascribed to the imine bond, proving the enolization of keto−enamine configurations in the excited state. Also, the ESIPT-induced isomerization did happen to TpBPy-COF. The N 1s signal in the dark was fitted into the C−N bond of keto−enamine and the C=N bond of the pyridinium moiety.[31,32] Upon irradiation, the relative intensity between the fitting peaks of the C−N and C=N bonds declined, revealing that the amount of partially enolized structures increased accordingly. The formed imine bonds were quantified to roughly estimate the tautomerization degree for TpPa-COF and TpBPy-COF (Table 1). Both COFs converted Keto into transition forms with approximately 35% enol−imine and 65% keto−enamine, indicative of the partial enolization of the excited COFs via ESIPT.

Transient absorption spectroscopy was carried out to study the excited states after nanosecond pulsed laser excitation across the COF series. Figure 3a shows the full transient absorption spectra of the three COFs dispersed in an aqueous solution. Note that TpBD-COF did not form a good dispersion after sonication, so it was excluded from the transient absorption measurements. To elucidate the uniqueness of charge transfer states for the partially enolized COFs, the imine-linked PyBPy-COF was adopted as a control, which consisted of a pyrene

Table 1. Estimation of Keto−Enamine (K) and Enol−Imine (E) Moieties in the Tautomers of TpPa-COF and TpBPy-COF through the Analysis of In Situ XPS Spectra (Figure 2c)

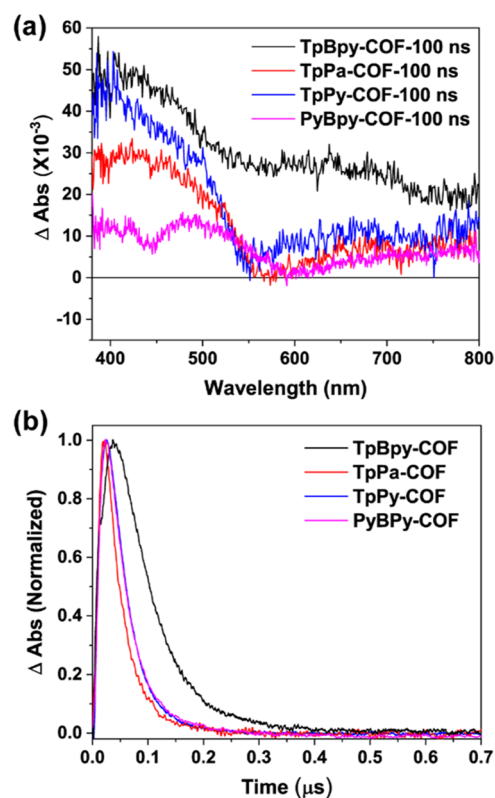|	C−N (%)	C=N (%)	K (%)	E (%)
TpPa-COF (dark)	100	0	100	0
TpPa-COF (irradiation)	65.05	34.95	65.0	35.0
TpBPy-COF (dark)	49.6	50.4	99.2	0.8
TpBPy-COF (irradiation)	32.8	68.2	63.6	36.4

Figure 3. (a) Absorption difference spectra of TpBPy-COF, TpPa-COF, TpPy-COF, and PyBPy-COF obtained at 80 ns time delay after pulsed 355 nm laser excitation (7 mJ cm^{-2}) in water. (b) Normalized absorption differences monitored at 420 nm as a function of time for TpBPy-COF, TpPa-COF, TpPy-COF, and PyBPy-COF.

moiety as a donor and a bipyridine moiety as an acceptor. All of the COFs showed broad photoinduced visible absorption bands around 400−550 and 600−850 nm during the 80 ns delay. These bands were attributed to the exciton absorption in the transition states. It was worth noting that TpBPy-COF gave significant photoinduced absorption from 550 to 700 nm compared to TpPa-COF, TpPy-COF, and PyBPy-COF. This suggests that the excited state of TpBPy-COF is subjected to exciton dissociation. Figure 3b reveals that the transition state decays back to the ground state on a time scale of tens to hundreds of nanoseconds. The decay kinetics could be well fit to the single exponential model, from which the abstracted lifetime constants for TpPa-COF, TpPy-COF, and PyBPy-COF showed similar values of 35, 41, and 41 ns, respectively. TpBPy-COF showed a much longer lifetime of 76 ns than the other COFs. Especially compared to PyBPy-COF, the significantly extended lifetime of TpBPy-COF is attributed to the remarkable charge separation.
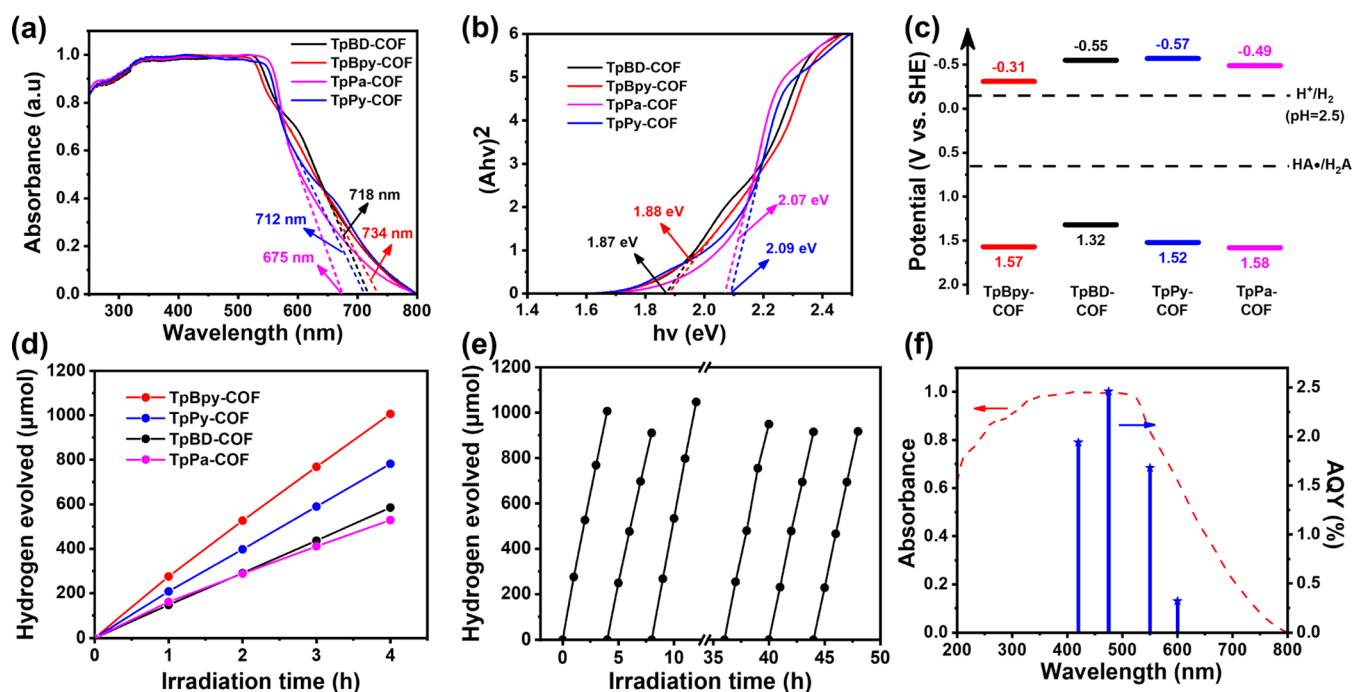
Figure 4. UV−vis−DRS spectra (a), Tauc plots (b), energy level diagram of band structures (c), and photocatalytic hydrogen evolution performance (d) of TpPa-COF, TpPy-COF, TpBD-COF, and TpBPy-COF. (e) 48 h photocatalytic cycles for TpBPy-COF. (f) Wavelength-dependent AQE for photocatalytic hydrogen evolution with TpBPy-COF.

Photocatalytic Hydrogen Evolution of Keto−Enamine-Linked COFs

As displayed in Figure 4a, the absorption edges in the UV−vis−DRS spectra appear at 675, 712, 718, and 734 nm for TpPa-COF, TpPy-COF, TpBD-COF, and TpBpy-COF, respectively, exhibiting a continuous red shift in the visible window. Tauc plots were used to calculate the optical band gaps of keto−enamine-linked COFs, which ranged from 1.87 to 2.09 eV (Figure 4b). The positive slopes of the Mott−Schottky plots demonstrated that the materials were n-type semiconductors (Supporting Information Figure S6). The flat-band potentials were then determined to be −0.31, −0.55, −0.57, and −0.49 V (vs SHE) for TpBPy-COF, TpBD-COF, TpPy-COF, and TpPa-COF, respectively. As the bottom of the conduction band (CB) could be approximately analogous to the flat band, it was applied to calculate the valence band (VB) with the optical band gaps. Thus, the energy band structures are confirmed, as displayed in Figure 4c. Also, the electrochemical band diagrams were established by cyclic voltammetry, showing similar oxidation potentials to VB and higher reduction potentials than CB (Supporting Information Figures S7 and S8) due to the need for extra energy against the interfacial barrier for charge injection. Thus, the optical band structures were applied to evaluate photocatalytic ability. All of the keto−enamine-linked COFs are thermodynamically favorable to reducing protons into H_2 when using ascorbic acid (AA) as the sacrificial electron donor.

Photocatalytic tests were carried out under visible irradiation ($\lambda > 420$ nm) in the presence of AA (0.1 M). The reaction solution was maintained at pH = 2.5 during photocatalysis. The static water contact angles of less than 60° indicated that all of the COFs showed similar wettability (Supporting Information Figure S9). Also, they appeared to have nonspecific morphologies and distinctly aggregated at the micrometer scale (Supporting Information Figure S10). The ultrafine Pt nanoparticles were photodeposited onto the COF solids to serve

as a cocatalyst. The uniform distribution on the COF matrix was observed, and the predominant sizes were around 2 nm (Supporting Information Figure S11). The contents of Pt were determined by ICP-AES to be 2.90 wt % for TpBD-COF, 2.88 wt % for TpBPy-COF, 2.93 wt % for TpPy-COF, and 2.90 wt % for TpPa-COF.

Upon exposure to visible irradiation, TpBPy-COF presented the highest hydrogen evolution rate (HER) of 25.2 mmol h^{-1} g^{-1} achieved at every 4 h interval over 48 h (Figure 4d,4e). Followed by TpBPy-COF, the HERs of TpPy-COF, TpBD-COF, and TpPa-COF declined dramatically from 19.5 to 14.6 and to 13.2 mmol h^{-1} g^{-1}. The stable keto−enamine linkages ensured the structural intactness of the recycled COFs during photocatalysis, which was evidenced by the measurement of PXRD and FT-IR (Supporting Information Figures S12 and S13). For comparison, amorphous analogues were synthesized by the aldimine reaction of Tp and diamines to estimate photocatalytic performances. The UV−vis absorption spectra of amorphous materials were similar to those of the corresponding COFs (Supporting Information Figure S14), while the HERs were only 8.6, 4.3, 4.0, and 3.5 mmol h^{-1} g^{-1} for poly(TpBPy), poly(TpPy), poly(TpBD), and poly(TpPa), respectively (Supporting Information Figure S15).

In the photophysical tests, TpBPy-COF afforded the largest photocurrent over the light on/off cycles (Supporting Information Figure S16) and the smallest resistance with the minimum radius of the semicircle in the Nyquist diagrams among the COFs (Supporting Information Figure S17). The best HER performances are also consistent with the longest charge separation lifetime determined by transient absorption spectroscopy. To further quantify the excellent photocatalytic activity of TpBPy-COF over the visible spectral distribution, apparent quantum efficiencies (AQEs) were measured to show a wavelength-dependent correlation (Figure 4f), and the maximum was 2.46% obtained at 475 nm.

Understanding of the ESIPT-Mediated Photocatalytic Mechanism

In general, ESIPT tautomers exhibit a drastic redistribution of the electronic density that makes the proton donor and acceptor stronger. After the photoinduced proton transfer, the strength of the formed H-bond between OH and C═N in K2E1 models was quantitively evaluated with the intrinsic bond strength index (IBSI) derived from the IGM formulation (Figure 5).[33] The
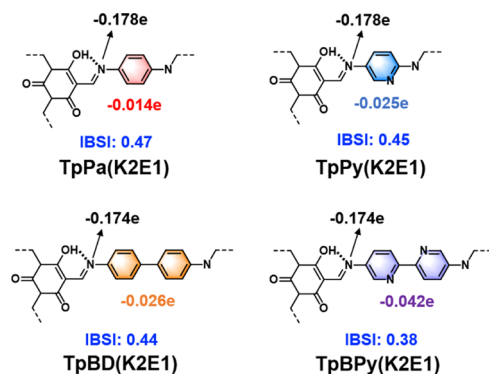

Figure 5. Computational calculations of the IBSI and fragment charges for the cutout models (K2E1) of isomerized TpPa-COF, TpPy-COF, TpBD-COF, and TpBPy-COF.

maximum IBSI for H···N bonding is 0.47 for the TpPa isomer (K2E1), followed by 0.45, 0.44, and 0.38 for TpPy, TpBD, and TpBPy isomers (K2E1), respectively. The same trend was achieved for the K1E2 and Enol isomers of different COF species (Supporting Information Tables S13). Given the electron push−pull effect, the atomic charge density was estimated for imine N and aromatic rings at the branches. It

was found that the low electron density on the aromatic rings such as the Pa moiety (−0.014e) led to the high electronegativity of imine N (−0.178e), thereby contributing to the strong hydrogen bonding in the K2E1 models. With all in mind, it is most likely that the partially enolized TpPa with the strongest H···N bonding allows for the improvement of enol−imine ring rigidity, which favors the formation of planar configuration and extended conjugation for the strong fluorescence emission.[34]

The electron−hole redistributions were computationally analyzed on the hexagonal models (Supporting Information Tables S14−S31 and Figures S18−S30). As shown in Figure 6, the real-space representation indicates that the forms of both Keto and Enol lead to local excitation without remarkable separation of electrons and holes. The charge separation of models could be quantitatively evaluated by the S-to-D ratio parameter,[35] of which S represents the overlap integral of hole−electron distribution and D means the distance between the centroid of the hole and the electron. Thus, the smaller S/D value reflects the smaller spatial overlap of electron accumulation and electron depletion, indicating the efficiency of electron−hole separation. The minimum S/D value of 0.03 A^{-1} is derived from partially enolized TpBPy-COF(K2E1), signifying the most efficient photogenerated electron−hole separation. This is consistent with the photocatalytic results that show that TpBPy-COF achieves optimal performance. In contrast, tautomer TpPa-COF(K2E1) bears the maximum S/D value of 72.73 A^{-1}, validating the possibility of electron−hole recombination. Thus, the radiative transition occurs on TpPa-COF, leading to strong fluorescence emission in the long-wavelength window.

The π-electron delocalization region in different isomers was estimated using the electron localization function (ELF).[36] As displayed in the ELF isosurface (isovalue = 0.39; Supporting
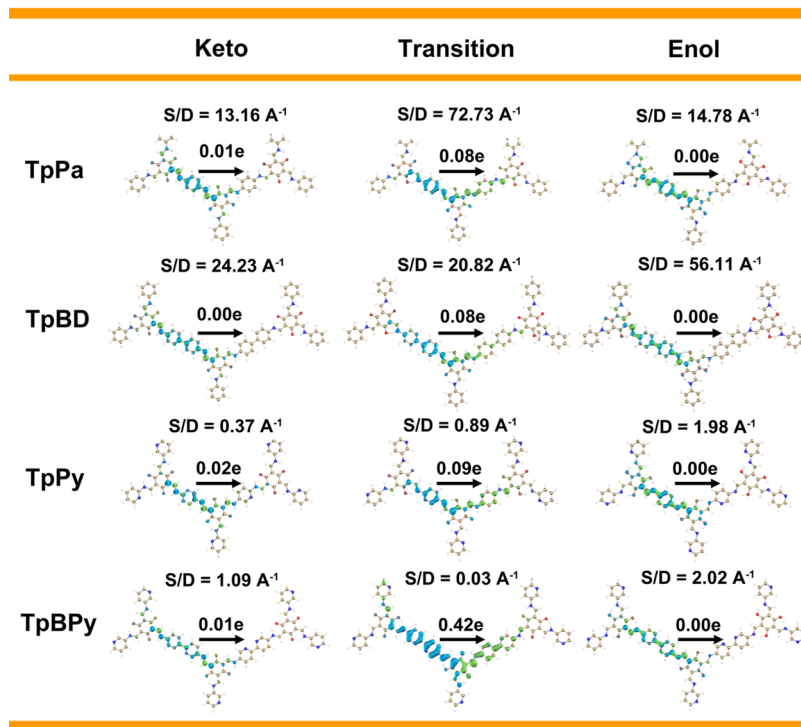

Figure 6. Electron−hole distributions for the hexagonal cutout models with different linkers (isovalue = 0.001, calculated on the TD-PBE0-D3/def2-SVP level). Blue and green regions represent the holes and electrons, respectively.
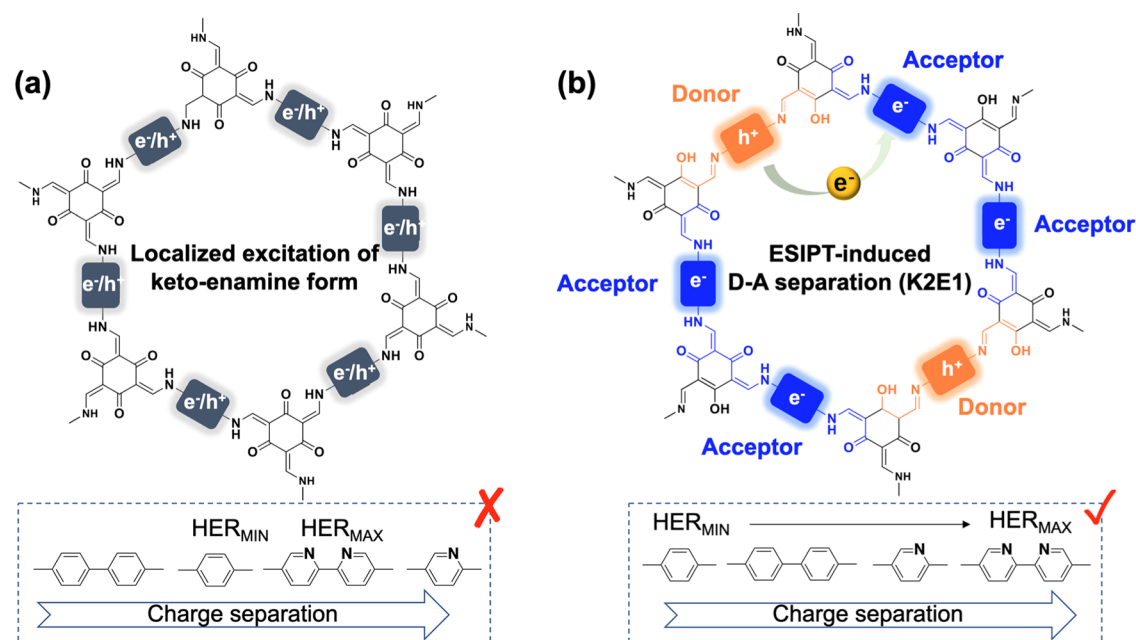
Figure 7. Illustration of the photoinduced charge separation for the COFs with different linkers including phenyl, biphenyl, pyridine, and bipyridine. (a) The inconsistent change between the photocatalytic HER and the predicted charge separation property for the Keto-form COFs in the excited state. (b) The identical changes in the HER and charge separation for ESIPT-induced photoisomer K2E1, of which the partially enolized moiety serves as a newly formed donor to reconstruct a spatially separated D−A system.

Information Figure S31), the delocalized conjugation of the Keto model was severely impeded due to the presence of phenyl-NH(enamine) and keto-C(enamine) moieties, which gave relatively low critical ELF values of 0.39 and 0.49, respectively. For the K2E1 isomer, the ESIPT-induced partial enolization remarkably enhanced π-conjugation at the same sites, showing increased critical ELF values of 0.47 and 0.70, respectively, corresponding to phenyl-N(imine) and enol−imine. Next, the inter-fragment charge transfer method was adopted to predict donor and acceptor moieties in different isomers.[37] As displayed in Figure 6, few electrons transfer between the two neighboring linkers in all of the Keto models. In contrast, the K2E1 isomers allow for the enhanced charge transfer. Among the four COFs, the partially enolized TpBPy-COF gave the largest charge value of 0.42e transferred from the enol−imine branch as a donor to the adjacent keto−enamine branch as an acceptor. This validates that ESIPT makes the excited COF rebuild a spatially separated donor−acceptor system. With PyBPy-COF as a control (Supporting Information Figure S32), charge transfer occurs between the adjacent Py (donor) and BPy (acceptor) units, accordingly limiting the range of electron delocalization and charge separation (Supporting Information Figure S30 and Table S32). The ESIPT triggers donor−acceptor separation in space, resulting in photoinduced electron migration in a large range. Therefore, the partially enolized structure facilitates an increase in the yield of separated charges and their lifetimes.

With all in mind, an insightful understanding of the ESIPT-involved photocatalytic mechanism is illustrated in Figure 7. Upon excitation, the intramolecular proton transfer occurs on the keto−enamine moiety, causing an in situ conversion into the partial enol−imine structure. The dominant isomer is the K2E1 form comprising two keto−enamine bonds and one enol−imine bond around a six-membered ring. Without ESIPT, the excitation of the keto−enamine isomer is localized on the linkers, shortening the charge transfer range. Upon photoisomerization, π-conjugation is extended to accumulate

electrons on the enol−imine-linked branch, rendering a new donor in the excited state.

Combined with the keto−enamine branch as an acceptor, the spatial separation of the donor and acceptor facilitates the photogenerated charge transfer between the neighboring edges of the framework. Indeed, the experimentally observed photocatalytic HER increases with the promotion of predicted charge separation in the K2E1 models. All of the Keto models exhibit significantly localized excitation, and the charge separation is the most remarkable using a pyridine linker, which noticeably disagrees with the experimental results. Therefore, ESIPT-induced photoisomerization plays a crucial role in understanding the structure-to-activity connection for the photocatalysis of keto−enamine-linked COFs.

CONCLUSIONS

In summary, we have demonstrated the ESIPT-induced photoisomerization of keto−enamine-linked COFs. The ESIPT process is responsible for the partial enolization of the keto−enamine linkage, directly leading to the extended π-conjugation and narrowed energy band gaps for light harvesting. Meanwhile, the π-electron density accordingly increases on the enol−imine-linked branch, which rebuilds a new donor−acceptor system with the keto−enamine-linked branch. We find that the charge transfer between the spatially separated donor and acceptor branches is long-range and more remarkable in the K2E1 models than in the Keto models without the need for an external donor. This can interpret the origin of the long-lived separated charges and enhanced photocatalytic H_2 evolution performances observed in the experiments. The ESIPT-caused photoisomerization from Keto to partial Enol is necessarily considered for a mechanistic insight into the photochemical dynamics. More intriguingly, the study on the charge separation state of ESIPT materials holds great promise for use in optoelectronic devices.

METHODS

Synthesis of Keto−Enamine-Linked COFs

All of the keto−enamine-linked COFs were synthesized by a solvothermal route. Typically, a Pyrex tube (10 mL) was charged Tp (21.0 mg, 0.1 mmol), BD (27.6 mg, 0.15 mmol), o-DCB (0.9 mL), n-BuOH (0.1 mL), and HOAc (6 M, 0.1 mL). The mixture was sonicated for 2 min and degassed through three freeze−pump−thaw cycles. Then, the tube was sealed off and kept in an oven at 120 °C for 3 days. After the reaction cooled to room temperature, the precipitate was collected by filtration and washed with THF and acetone several times. Then, the solid was extracted by a Soxhlet instrument with THF for 1 day and dried under vacuum at 40 °C for 24 h, affording TpBD-COF in 83% yield. The other COFs were prepared by a similar route, and the detailed recipes were as follows: TpBPy-COF: Tp (21.0 mg, 0.1 mmol), Bp (27.9 mg, 0.15 mmol), mesitylene (0.5 mL), dioxane (0.5 mL), and HOAc (6 M, 0.1 mL). The yield was 80%. TpPy-COF: Tp (21.0 mg, 0.1 mmol), Py (16.4 mg, 0.15 mmol), dioxane (0.75 mL), and HOAc (3 M, 0.25 mL). The yield was 79%. TpPa-COF: Tp (21.0 mg, 0.1 mmol), Pa (16.4 mg, 0.15 mmol), mesitylene (0.5 mL), dioxane (0.5 mL), and HOAc (3 M, 0.1 mL). The yield was 81%.

Photocatalytic Measurement

The H_2 evolution test was performed in a top-irradiation reaction vessel of a Labsolar 6A system (Beijing Perfect Light Technology Co., Ltd.) under irradiation of a 300 W Xe lamp equipped with a cutoff filter ($\lambda \geq$ 420 nm). H_2 was analyzed by gas chromatography (Techcomp GC7900). H_2PtCl_6 aqueous solution (3.86 mM, 0.405 mL) was added for loading 3 wt % Pt onto the COF solid (10 mg) by photodeposition. Photocatalysis was carried out by dispersing 10 mg of the photocatalyst in 100 mL of water with ascorbic acid (0.1 M) as the sacrificial electron donor. The pH value of the reaction solution was measured to be 2.5 during photocatalysis. The mixture was evacuated several times to remove air completely before irradiation. The reaction temperature was kept at 8 °C by flowing water.

ASSOCIATED CONTENT

ⓢ Supporting Information

The Supporting Information is available free of charge at https://pubs.acs.org/doi/10.1021/jacsau.3c00554.

> Materials and methods; pore size distributions; FT-IR spectra; Mott−Schottky plots; cyclic voltammetry; UV−vis−NIR spectra; solid-state CP/MAS ^{13}C NMR spectra; PXRD patterns; N_2 sorption isotherms; TEM images; and calculation details (PDF)

AUTHOR INFORMATION

Corresponding Authors

Ke Hu − Department of Chemistry, Fudan University, Shanghai 200438, China; ⓞ orcid.org/0000-0002-0240-7192; Email: khu@fudan.edu.cn

Jia Guo − State Key Laboratory of Molecular Engineering of Polymers, Department of Macromolecular Science, Fudan University, Shanghai 200438, China; ⓞ orcid.org/0000-0003-4869-9992; Email: guojia@fudan.edu.cn

Authors

Weijun Weng − State Key Laboratory of Molecular Engineering of Polymers, Department of Macromolecular Science, Fudan University, Shanghai 200438, China

Zheng Lin − State Key Laboratory of Molecular Engineering of Polymers, Department of Macromolecular Science, Fudan University, Shanghai 200438, China

Hualei Zhang − State Key Laboratory of Molecular Engineering of Polymers, Department of Macromolecular Science, Fudan University, Shanghai 200438, China

Fushuang Niu − Department of Chemistry, Fudan University, Shanghai 200438, China

Changchun Wang − State Key Laboratory of Molecular Engineering of Polymers, Department of Macromolecular Science, Fudan University, Shanghai 200438, China; ⓞ orcid.org/0000-0003-3183-2160

Complete contact information is available at:
https://pubs.acs.org/10.1021/jacsau.3c00554

Author Contributions

[§]W.W. and Z.L. contributed equally to this paper. CRediT: **Weijun Weng** investigation, writing-original draft, writing-review & editing; **Zheng Lin** investigation, writing-review & editing; **Hualei Zhang** investigation; **Fushuang Niu** investigation; **Changchun Wang** funding acquisition, resources, writing-review & editing; **Ke Hu** funding acquisition, investigation, methodology, writing-review & editing; **Jia Guo** conceptualization, funding acquisition, project administration, resources, supervision, writing-review & editing.

Notes

The authors declare no competing financial interest.

ACKNOWLEDGMENTS

REFERENCES

(1) Sedgwick, A. C.; Wu, L.; Han, H.-H.; Bull, S. D.; He, X.-P.; James, T. D.; Sessler, J. L.; Tang, B. Z.; Tian, H.; Yoon, J. Excited-state intramolecular proton-transfer (ESIPT) based fluorescence sensors and imaging agents. *Chem. Soc. Rev.* **2018**, *47*, 8842−8880.

(2) Côté, A. P.; Benin, A. I.; Ockwig, N. W.; Matzger, A. J.; O'Keeffe, M.; Yaghi, O. M. Porous, Crystalline, Covalent Organic Frameworks. *Science* **2005**, *310*, 1166−1170.

(3) Geng, K.; He, T.; Liu, R.; Dalapati, S.; Tan, K. T.; Li, Z.; Tao, S.; Gong, Y.; Jiang, Q.; Jiang, D. Covalent Organic Frameworks: Design, Synthesis, and Functions. *Chem. Rev.* **2020**, *120*, 8814−8933.

(4) Nguyen, H. L.; Hanikel, N.; Lyle, S. J.; Zhu, C.; Proserpio, D. M.; Yaghi, O. M. A Porous Covalent Organic Framework with Voided Square Grid Topology for Atmospheric Water Harvesting. *J. Am. Chem. Soc.* **2020**, *142*, 2218−2221.

(5) Ying, Y.; Tong, M.; Ning, S.; Ravi, S. K.; Bo Peh, S.; Tan, S. C.; Pennycook, S. J.; Zhao, D. Ultrathin Two-Dimensional Membranes Assembled by Ionic Covalent Organic Nanosheets with Reduced Apertures for Gas Separation. *J. Am. Chem. Soc.* **2020**, *142*, 4472−4480.

(6) Sun, Q.; Tang, Y.; Aguila, B.; Wang, S.; Xiao, F.-S.; Thallapally, P. K.; Al-Enizi, A. M.; Nafady, A.; Ma, S. Reaction Environment Modification in Covalent Organic Frameworks for Catalytic Performance Enhancement. *Angew. Chem., Int. Ed.* **2019**, *58*, 8670−8675.

(7) Hu, Y.; Huang, W.; Wang, H.; He, Q.; Zhou, Y.; Yang, P.; Li, Y.; Li, Y. Metal-Free Photocatalytic Hydrogenation Using Covalent Triazine Polymers. *Angew. Chem., Int. Ed.* **2020**, *59*, 14378.

(8) Hu, X.; Zhan, Z.; Zhang, J.; Hussain, I.; Tan, B. Immobilized covalent triazine frameworks films as effective photocatalysts for hydrogen evolution reaction. *Nat. Commun.* **2021**, *12*, No. 6596.

(9) DeBlase, C. R.; Silberstein, K. E.; Truong, T.; Abruña, H. D.; Dichtel, W. R. β-Ketoenamine-Linked Covalent Organic Frameworks

Capable of Pseudocapacitive Energy Storage. *J. Am. Chem. Soc.* **2013**, *135*, 16821−16824.

(10) Hu, X.; Jian, J.; Fang, Z.; Zhong, L.; Yuan, Z.; Yang, M.; Ren, S.; Zhang, Q.; Chen, X.; Yu, D. Hierarchical assemblies of conjugated ultrathin COF nanosheets for high-sulfur-loading and long-lifespan lithium−sulfur batteries: Fully-exposed porphyrin matters. *Energy Storage Mater.* **2019**, *22*, 40−47.

(11) Niu, C.; Luo, W.; Dai, C.; Yu, C.; Xu, Y. High-Voltage-Tolerant Covalent Organic Framework Electrolyte with Holistically Oriented Channels for Solid-State Lithium Metal Batteries with Nickel-Rich Cathodes. *Angew. Chem., Int. Ed.* **2021**, *60*, 24915−24923.

(12) Jin, E.; Asada, M.; Xu, Q.; Dalapati, S.; Addicoat, M. A.; Brady, M. A.; Xu, H.; Nakamura, T.; Heine, T.; Chen, Q.; Jiang, D. Two-dimensional sp^2 carbon−conjugated covalent organic frameworks. *Science* **2017**, *357*, 673−676.

(13) Wang, X.; Chen, L.; Chong, S. Y.; Little, M. A.; Wu, Y.; Zhu, W.; Clowes, R.; Yan, Y.; Zwijnenburg, M. A.; Sprick, R. S.; Cooper, A. I. Sulfone-containing covalent organic frameworks for photocatalytic hydrogen evolution from water. *Nat. Chem.* **2018**, *10*, 1180−1189.

(14) Pachfule, P.; Acharjya, A.; Roeser, J.; Langenhahn, T.; Schwarze, M.; Schomäcker, R.; Thomas, A.; Schmidt, J. Diacetylene Function-alized Covalent Organic Framework (COF) for Photocatalytic Hydrogen Generation. *J. Am. Chem. Soc.* **2018**, *140*, 1423−1427.

(15) Chen, W.; Wang, L.; Mo, D.; He, F.; Wen, Z.; Wu, X.; Xu, H.; Chen, L. Modulating Benzothiadiazole-Based Covalent Organic Frameworks via Halogenation for Enhanced Photocatalytic Water Splitting. *Angew. Chem., Int. Ed.* **2020**, *59*, 16902−16909.

(16) Zhou, T.; Wang, L.; Huang, X.; Unruangsri, J.; Zhang, H.; Wang, R.; Song, Q.; Yang, Q.; Li, W.; Wang, C.; Takahashi, K.; Xu, H.; Guo, J. PEG-stabilized coaxial stacking of two-dimensional covalent organic frameworks for enhanced photocatalytic hydrogen evolution. *Nat. Commun.* **2021**, *12*, No. 3934.

(17) Mi, Z.; Zhou, T.; Weng, W.; Unruangsri, J.; Hu, K.; Yang, W.; Wang, C.; Zhang, K. A. I.; Guo, J. Covalent Organic Frameworks Enabling Site Isolation of Viologen-Derived Electron-Transfer Mediators for Stable Photocatalytic Hydrogen Evolution. *Angew. Chem., Int. Ed.* **2021**, *60*, 9642−9649.

(18) Vyas, V. S.; Haase, F.; Stegbauer, L.; Savasci, G.; Podjaski, F.; Ochsenfeld, C.; Lotsch, B. V. A tunable azine covalent organic framework platform for visible light-induced hydrogen generation. *Nat. Commun.* **2015**, *6*, No. 8508.

(19) Wei, S.; Zhang, F.; Zhang, W.; Qiang, P.; Yu, K.; Fu, X.; Wu, D.; Bi, S.; Zhang, F. Semiconducting 2D Triazine-Cored Covalent Organic Frameworks with Unsubstituted Olefin Linkages. *J. Am. Chem. Soc.* **2019**, *141*, 14272−14279.

(20) Meier, C. B.; Clowes, R.; Berardo, E.; Jelfs, K. E.; Zwijnenburg, M. A.; Sprick, R. S.; Cooper, A. I. Structurally Diverse Covalent Triazine-Based Framework Materials for Photocatalytic Hydrogen Evolution from Water. *Chem. Mater.* **2019**, *31*, 8830−8838.

(21) Feng, X.; Liu, L.; Honsho, Y.; Saeki, A.; Seki, S.; Irle, S.; Dong, Y.; Nagai, A.; Jiang, D. High-Rate Charge-Carrier Transport in Porphyrin Covalent Organic Frameworks: Switching from Hole to Electron to Ambipolar Conduction. *Angew. Chem., Int. Ed.* **2012**, *51*, 2618−2622.

(22) Kandambeth, S.; Mallick, A.; Lukose, B.; Mane, M. V.; Heine, T.; Banerjee, R. Construction of Crystalline 2D Covalent Organic Frameworks with Remarkable Chemical (Acid/Base) Stability via a Combined Reversible and Irreversible Route. *J. Am. Chem. Soc.* **2012**, *134*, 19524−19527.

(23) Mamada, M.; Inada, K.; Komino, T.; W, J. P., Jr.; Nakanotani, H.; Adachi, C. Highly Efficient Thermally Activated Delayed Fluorescence from an Excited-State Intramolecular Proton Transfer System. *ACS Cent. Sci.* **2017**, *3*, 769−777.

(24) Traxler, M.; Gisbertz, S.; Pachfule, P.; Schmidt, J.; Roeser, J.; Reischauer, S.; Rabeah, J.; Pieber, B.; Thomas, Arne. Acridine-Functionalized Covalent Organic Frameworks (COFs) as Photo-catalysts for Metallaphotocatalytic C−N Cross-Coupling. *Angew. Chem., Int. Ed.* **2022**, *61*, No. e202117738.

(25) Han, X.; Zhang, J.; Huang, J.; Wu, X.; Yuan, D.; Liu, Y.; Cui, Y. Chiral induction in covalent organic frameworks. *Nat. Commun.* **2018**, *9*, No. 1294, DOI: 10.1038/s41467-018-03689-9.

(26) Biswal, B. P.; Chandra, S.; Kandambeth, S.; Lukose, B.; Heine, T.; Banerjee, R. Mechanochemical Synthesis of Chemically Stable Isoreticular Covalent Organic Frameworks. *J. Am. Chem. Soc.* **2013**, *135*, 5328−5331.

(27) Chandra, S.; Kundu, T.; Dey, K.; Addicoat, M.; Heine, T.; Banerjee, R. Interplaying Intrinsic and Extrinsic Proton Conductivities in Covalent Organic Frameworks. *Chem. Mater.* **2016**, *28*, 1489−1494.

(28) Wang, R.; Kong, W.; Zhou, T.; Wang, C.; Guo, J. Organobase modulated synthesis of high-quality β-ketoenamine-linked covalent organic frameworks. *Chem. Commun.* **2021**, *57*, 331−334.

(29) Barboza, C. A.; Gawrys, P.; Banasewicz, M.; Kozankiewicz, B.; Sobolewski, A. L. Substituent effects on the photophysical properties of tris(salicylideneanilines). *Phys. Chem. Chem. Phys.* **2021**, *23*, 1156−1164.

(30) Khattak, A. M.; Ghazi, Z. A.; Liang, B.; Khan, N. A.; Iqbal, A.; Li, L.; Tang, Z. A redox-active 2D covalent organic framework with pyridine moieties capable of faradaic energy storage. *J. Mater. Chem. A* **2016**, *4*, 16312−16317.

(31) Sun, Q.; Aguila, B.; Perman, J.; Nguyen, N.; Ma, S. Flexibility Matters: Cooperative Active Sites in Covalent Organic Framework and Threaded Ionic Polymer. *J. Am. Chem. Soc.* **2016**, *138*, 15790−15796.

(32) Zhao, X.; Pachfule, P.; Li, S.; Langenhahn, T.; Ye, M.; Schlesiger, C.; Praetz, S.; Schmidt, J.; Thomas, A. Macro/Microporous Covalent Organic Frameworks for Efficient Electrocatalysis. *J. Am. Chem. Soc.* **2019**, *141*, 6623−6630.

(33) Klein, J.; Khartabil, H.; Boisson, J.; Contreras-García, J.; Piquemal, J.; Hénon, E. New Way for Probing Bond Strength. *J. Phys. Chem. A* **2020**, *124*, 1850−1860.

(34) Li, X.; Gao, Q.; Wang, J.; Chen, Y.; Chen, Z.; Xu, H.; Tang, W.; Leng, K.; Ning, G.; Wu, J.; Xu, Q.; Quek, S. Y.; Lu, Y.; Loh, K. P. Tuneable near white-emissive two-dimensional covalent organic frameworks. *Nat. Commun.* **2018**, *9*, No. 2335.

(35) Yuan, J.; Yuan, Y.; Tian, X.; Liu, Y.; Sun, J. Insights into the photobehavior of fluorescent oxazinone, quinazoline, and difluorobor-on derivatives: Molecular design based on the structure−property relationships. *J. Phys. Chem. C* **2017**, *121*, 8091−8108.

(36) Becke, A. D.; Edgecombe, K. E. A simple measure of electron localization in atomic and molecular systems. *J. Chem. Phys.* **1990**, *92*, 5397−5403.

(37) Gao, Z.; Chen, S.; Bai, Y.; Wang, M.; Liu, X.; Yang, W.; Li, W.; Ding, X.; Yao, J. A new perspective for evaluating the photoelectric performance of organic−inorganic hybrid perovskites based on the DFT calculations of excited states. *Phys. Chem. Chem. Phys.* **2021**, *23*, 11548−11556.